Geophys. J. Int. (2005) **163,** 931–943 doi: 10.1111/j.1365-246X.2005.02789.x

Electrical structure of the crust below the Deccan Flood Basalts (India), inferred from magnetotelluric soundings

B. Prasanta K. Patro,[1,2] Heinrich Brasse,[2] S. V. S. Sarma[1] and T. Harinarayana[1]

[1]*National Geophysical Research Institute, Uppal Road, Hyderabad,* 500 007, *India. E-mail: patrobpk@rediffmail.com*
[2]*Fachrichtung Geophysik, FU Berlin, Malteserstr.* 74-100, 12249 *Berlin, Germany*

Accepted 2005 August 15. Received 2005 August 12; in original form 2004 June 2

SUMMARY

The Indian shield has experienced major stable continental region (SCR) earthquakes in the recent past, which occurred in the Deccan Volcanic Province. Until now the deeper crust below the Deccan traps, where thick basaltic layers cover large areas of the Indian shield, remains poorly understood. A magnetotelluric (MT) study covering a broad period range was conducted along a N–S running profile of 330 km length to achieve more insights into the nature of the crustal electrical structure below the flood basalts. After dimensionality analysis and decomposition, 2-D inversions for TE and TM modes were carried out. The basalt cover, characterized by at first glance surprisingly low electrical resistivities, is found to have an average thickness of 400 m with the exception of central parts of the profile where it reaches up to 700 m. The crust is in general highly resistive, but several subvertical zones of enhanced conductivity were delineated in the middle-to-lower crust, which are tentatively explained as images of hidden, partly reactivated faults/fractures of the Precambrian basement. Sensitivity analysis indicates a high resolution of these features. An alternative approach incorporating macro-anisotropy is additionally considered and corresponding 2-D anisotropic forward modelling confirms the existence of successions of conductive dykes in the deep crust.

Key words: anisotropy, Deccan traps, magnetotellurics, 2-D inversion.

1 INTRODUCTION

The Deccan Volcanic Province (DVP) of western India is one of the great igneous provinces on Earth. Vast amounts of basalts erupted some 65 Ma years ago at the Upper Cretaceous–Tertiary boundary, commonly believed to be due to the northward passage of the Indian plate over the Reunion hotspot (Duncan & Pyle 1988). The basaltic layers (traps) cover an area of approx. 500 000 km^2 of the Indian peninsular shield, reaching average thicknesses of several hundred metres up to 2 km. K-Ar geochronology and magnetostratigraphy, coupled with palaeontological analysis, led Courtillot *et al.* (1986) to propose that the Deccan flood basalt province had erupted in less than 1 Ma. The flood basalts are of tholeiitic composition and consists of different flows, which mainly comprise massive, vesicular, amygdoidal basalt, tuff and breccia. A drill hole in the eastern part of the DVP passed through eight flows of tholeiitic basalts of thickness 338 m with 8 m of intratrappean and reached the basement at a depth of 348 m (Gupta & Dwivedy 1996). The province is associated with several continental scale and smaller rift zones (Biswas 1982, 1987; Sheth & Chandrasekharam 1997), namely the West Coast belt, the E–W trending Narmada–Satpura–Tapi graben–horst–graben system, the Cambay, Kachchh, Mahanadi and Godavari rifts. These rift basins run along major Precambrian tectonic trends in the ancient Indian shield and formed at different times during the Mesozoic (Biswas 1982, 1987).

The Indian shield was believed to be aseismic and stable but the occurrence of recent stable continental region (SCR) earthquakes has opened up several challenging problems particularly in relation to the increased sesimicity in the Deccan trap region. Three major SCR earthquakes (Koyna 1967; Latur 1993; Jabalpur 1997) of magnitude $M > 6.0$ that occurred in the Indian peninsular shield over the last decades were located in the DVP. SCR seismicity normally constitutes a very small percentage (5 per cent) of total seismicity and most of the SCR activity (95 per cent) occurs in extended regions like rift zones, failed margins, etc. (Johnston & Kanter 1990). However, the effects of the SCR seismicity have been found to be devastating, for example, the 1993 Latur earthquake caused enormous loss of life (11 000 deaths) and property (Gupta *et al.* 1993). It is thus essential to understand the seismogenic processes relevant to SCRs and also to identify possible zones vulnerable for occurrence of such events.

Several geophysical studies were carried out in the greater area of DVP including gravity (Kailasam *et al.* 1972; Krishna Brahmam & Negi 1973; Tiwari *et al.* 2001), deep seismic sounding (Kaila *et al.* 1981a,b) and magnetotellurics (Gokarn *et al.* 1992). Krishna Brahmam & Negi (1973) interpreted a NW–SE trending gravity 'low' passing through Kurduwadi as a subtrappean rift and named it 'Kurduwadi' rift. But later studies conducted in this region (Tiwari *et al.* 2001; Gokarn *et al.* 1992) do not indicate any rift related features like thick sediments, faults, etc. Gravity studies by

Tiwari *et al.* (2001) suggested the 'Kurduwadi low' could be attributed mainly to the emplacement of low-density (2.62 gm cm^{-3}) material in the upper crust such as granitic bodies along fracture/shear zones. The magnetotelluric study by Gokarn *et al.* (1992) inferred a mid-crustal conductor at depths varying between 12 and 18 km, which they associated with the Conrad discontinuity. MT investigations in the Latur earthquake epicentral area (Sarma *et al.* 1994; Gupta *et al.* 1996) revealed the presence of a high-conductivity zone at shallow depth range of 6–10 km and the thickness of basalt ranges from 300 to 400 m. MT study in central India by Gokarn *et al.* (2001) and Patro *et al.* (2005) delineated conductive features of about 4–30 Ωm in a depth range between 10 and 35 km and interpreted this enhanced conductivity to be due to the fluid present in the fractures associated with the fault. A recent MT study carried out by Sarma *et al.* (2004) in the Koyna seismic zone identified block structures in the crustal column and they also inferred that the Koyna fault zone is characterized by a moderately conductive feature. Results from DC geoelectrical soundings suggest the trap thickness to vary between 220 and 1200 m (Kailasam *et al.* 1976; Bhaskar Rao *et al.* 1995), but information about deeper structures could not be obtained because of limitation of the employed field configuration. Until now only a few academic MT surveys were carried out to image beneath basalt covered areas in other parts of the world (e.g. Prieto *et al.* 1985; Warren & Srnka 1992). Many commercial surveys have been done in this context in US, Turkey, Libya and elsewhere.

In an effort to determine the thickness of the Deccan Trap rocks in the Koyna area, aeromagnetic data were acquired on 13 short profiles, each about 100 km long and spaced at 4 km (Negi *et al.* 1983). Two major features were interpreted from the aeromagnetic maps. The first is a broad NNE–SSW zone, extending from north of Koyna dam to 40 km to the SSW; the other is a NW–SE anomaly along the upper reaches of Warna river. Recently aeromagnetic data in the area between 17° to 24°N, 78° to 88°E were analysed to understand various tectonic blocks of the region (Rajan & Anand 2003). However, aeromagnetic data have not been collected to the west of this region above the trap cover, which constitutes a difficult target for aeromagnetic studies.

For the purpose of the present investigations, wide-band magnetotelluric soundings were carried out in the Deccan plateau region (Fig. 1) along a profile across significant gravity anomalies like Kurduwadi low and Sangole high. The study was aimed to understand the electrical nature of the crustal column below the trap region. A total of 41 single site MT stations covering a period range from 0.001 to 1000 s were set up along a profile of 330 km length with a station interval of 5–7 km during 1998 and 1999 field campaigns. Metronix GMS05 broad-band systems were used for data acquisition. The time-series were edited off-line to remove sections contaminated by noise and then analysed using robust processing technique. Unfortunately data of the vertical magnetic field (Hz) were very often noisy and could not be considered here.

Typical MT transfer functions (site SP25) are presented in Fig. 2. They show a moderately resistive surface layer at short periods, and the steep rise of apparent resistivities ρ_a (and according low phase values ϕ) at longer periods, reflecting the basement. At periods $T > 1$ s the curves split, indicating a deep-seated electrical anomaly. Such behaviour is characteristic for nearly all sites along the profile. Qualitative insights into the variations of subsurface electrical structure along the traverse may be seen from the ρ_a and ϕ versus frequency pseudo-sections (see later in Fig. 6). The pseudo-sections of ρ_{xy} as well as ρ_{yx} show that the shallow layers are moderately resistive (about 50 Ωm) representing the Deccan traps. These are underlain by a highly resistive basement all along the traverse.

2 DIMENSIONALITY AND REGIONAL STRIKE ANALYSIS

From the magnetotelluric impedance tensor a rotationally invariant skewness or skew (Swift 1967) as a measure for deviation from 1-D

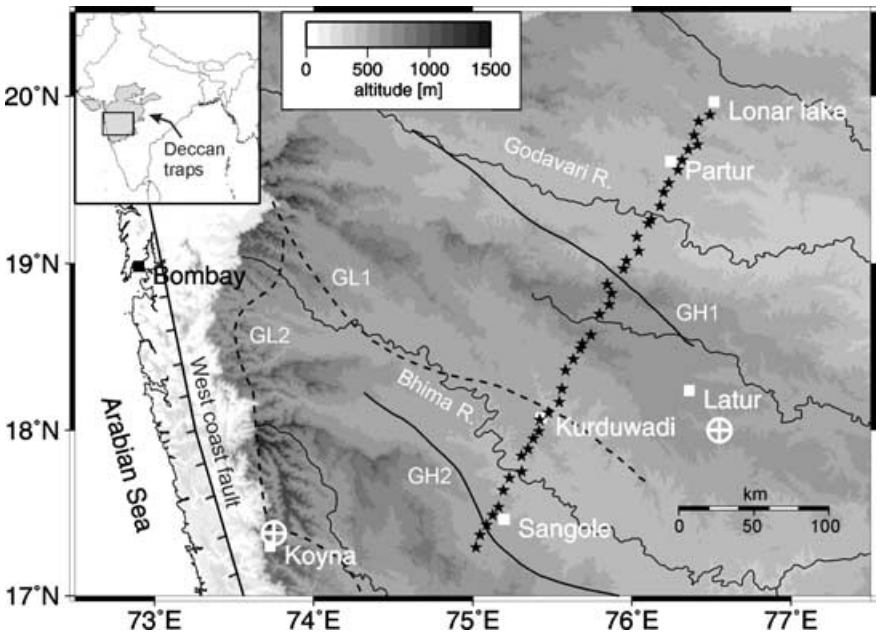

Figure 1. Location of magnetotelluric sites (stars) in the Deccan Volcanic Province (DVP). Also shown are the traces of gravity lows (GL) and highs (GH) redrawn from Kailasam *et al.* (1972). ⊕ denotes the location of earthquake epicentres with $M > 6.0$ (from Gupta *et al.* 2002). West coast fault is redrawn from Biswas (1982).

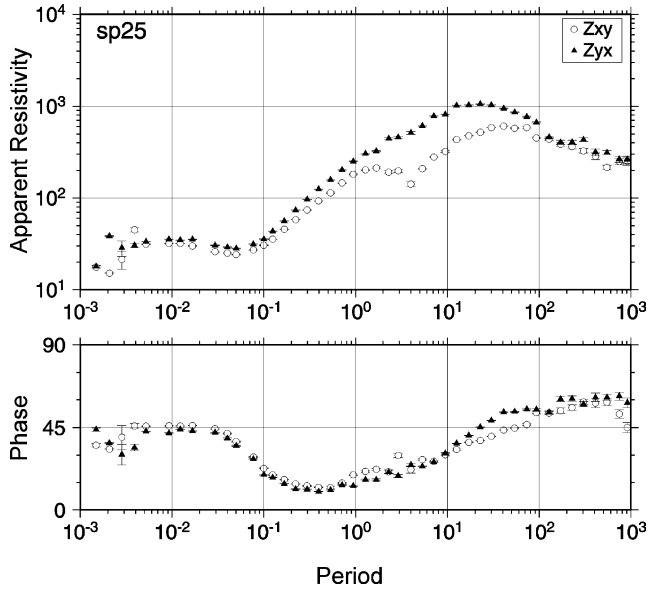

Figure 2. Example of transfer functions (apparent resistivities and phases) at site SP25 in the DVP, as measured in the original N–S, E–W coordinate frame.

or 2-D structures is derived. Fig. 3 (top) shows the skew-period section along the profile. For periods below 1 s, skew values are <0.1, indicating a 1-D/2-D nature of the top layers, but at longer periods marginally higher values (<0.2) are observed, with the exception of sites SP10–SP14, where a higher value of 0.3–0.4 is noticed. Since magnetotelluric impedances are frequently distorted by accumulation of electrical charges along near-surface inhomogeneities, we have also calculated the phase-sensitive skew (Fig. 3, centre) taking into account a superposition model with a shallow 3-D structure overlying a regional 2-D structure, which is less prone to static effects (Bahr 1988). It shows slightly higher values especially in the frequency range from 1 to 10 s, which we attribute to poor data quality due to the influence of noise in the so-called dead band in the spectrum of geomagnetic variations. Altogether, the skew parameter generally shows values between 0 and 0.2 with an increase at a few locations. Keeping this in mind the 2-D approach is applied.

The occurrence of near-surface anomalies also poses a problem for the determination of the true regional strike direction. In our particular case we have followed two different approaches by Smith (1997) and McNeice & Jones (2001). In the case of Smith's approach the impedances at each site are fitted for distortion parameters and strikes frequency by frequency, and a single best strike angle at the site is determined. Then it calculates a single best strike direction for the whole set of sites. On the other hand McNeice and Jones' approach is an extension to the Groom–Bailey decomposition in which a global minimum is sought to determine the most suitable strike direction and the telluric distortion parameters for a range of frequencies and for the set of sites. Both approaches resulted in nearly the same strike angle for most of the sites which varies from 25° to 45°. A significant difference is observed at a few sites near Kurduwadi (Fig. 3). This corresponds to the region where the skew value is relatively high, thus the assumption of a 2-D background model is violated here.

The approaches according to Smith and of McNeice and Jones yielded similar best strike values of 25° and 30° respectively. Taking the inherent 90° ambiguity into consideration we have rotated the data of sites SP1–SP18 by −50° and the rest by −65°. The derived strike direction is in general agreement with the gravity anomalies and the geology. The electric field which is oriented parallel to assumed geoelectric strike is assigned as TE mode and the magnetic field as TM mode.

3 MODELLING RESULTS

3.1 Characterization of the volcanic layer

The 1-D at short periods permits a 1-D modelling approach (Patro 2002). Fig. 4 (top) shows the inversion results incorporating a Marquardt-style inversion technique, implemented in the Geotools software package (1997). Both average impedances $Z_{av} = (Z_{xy} - Z_{yx})/2$ (Berdichevsky & Dmitriev 1976) and effective impedance $Z_{\det} = (Z_{xx}Z_{yy} - Z_{xy}Z_{yx})^{1/2}$ (where Z_{xx}, Z_{yy} are diagonal elements and Z_{xy}, Z_{yx} are antidiagonal elements of the impedance tensor) (Ranganayaki 1984) were inverted, giving similar results. Additionally, the steep gradient of nearly 45° of the apparent resistivity curves provides a simple (crude) estimate of surface conductance S according to (e.g. Berdichevsky & Dimitriev 2002):

$$S \approx \frac{1}{\mu_0 |Z|},$$

where μ_0 is the free space permeability and Z is the magnetotelluric impedance, measured in (mV km^{-1})/nT. This leads to:

$$S \approx \left(\frac{T_P}{2\pi \mu_0 \rho_a(T_P)} \right)^{1/2},$$

with P indicating a point on the 45°-rise of the ρ_a(T)-curve. A possible correction term accounting for the finite (but unknown) resistivity of the basement is omitted here. Sites SP5, SP11 and SP36 were not considered for the above estimation, because of noise contamination of high-frequency data. This yields conductancies of 5–20 Siemens along the profile (Fig. 4, bottom), in accordance with 1-D modelling results.

The trap resistivity is at first glance surprisingly low with 35–40 Ωm along the profile. We attribute this to deep-reaching weathering of the basaltic layers, considering the time of eruption (65 Ma ago) and/or intercalated thin sedimentary layers between the individual flows. The depth to the basement undulates around 400 m, with some exception near SP23, where it reaches up to 700 m.

3.2 Deep structure

The non-linear conjugate gradient algorithm of Rodi and Mackie (2001) was applied to carry out 2-D inversion. TE and TM mode data in a period range between 0.01 and 300 s were used as input data. In the algorithm the regularization parameter τ plays a significant role, controlling the balance between data fit and model roughness. In order to find an appropriate τ, the inversion was carried out several times with different τ values. If the resulting rms errors are plotted against model norm or roughness, a typical L-shaped trade-off curve (Hansen 1998) should be obtained and the preferable τ should lie in the knee of the curve. In the magnetotelluric case, however, the L-shape is often not clearly expressed (Fig. 5, see also comments in Schwalenberg *et al.* (2002)). For the final model we have chosen $\tau = 15$. Other computations comprised settings of error floors and horizontal/vertical weighting factors as well as evaluation of convergence behaviour (for the model in Fig. 6a the number of iterations was 114, with a homogeneous half-space of 100 Ωm as

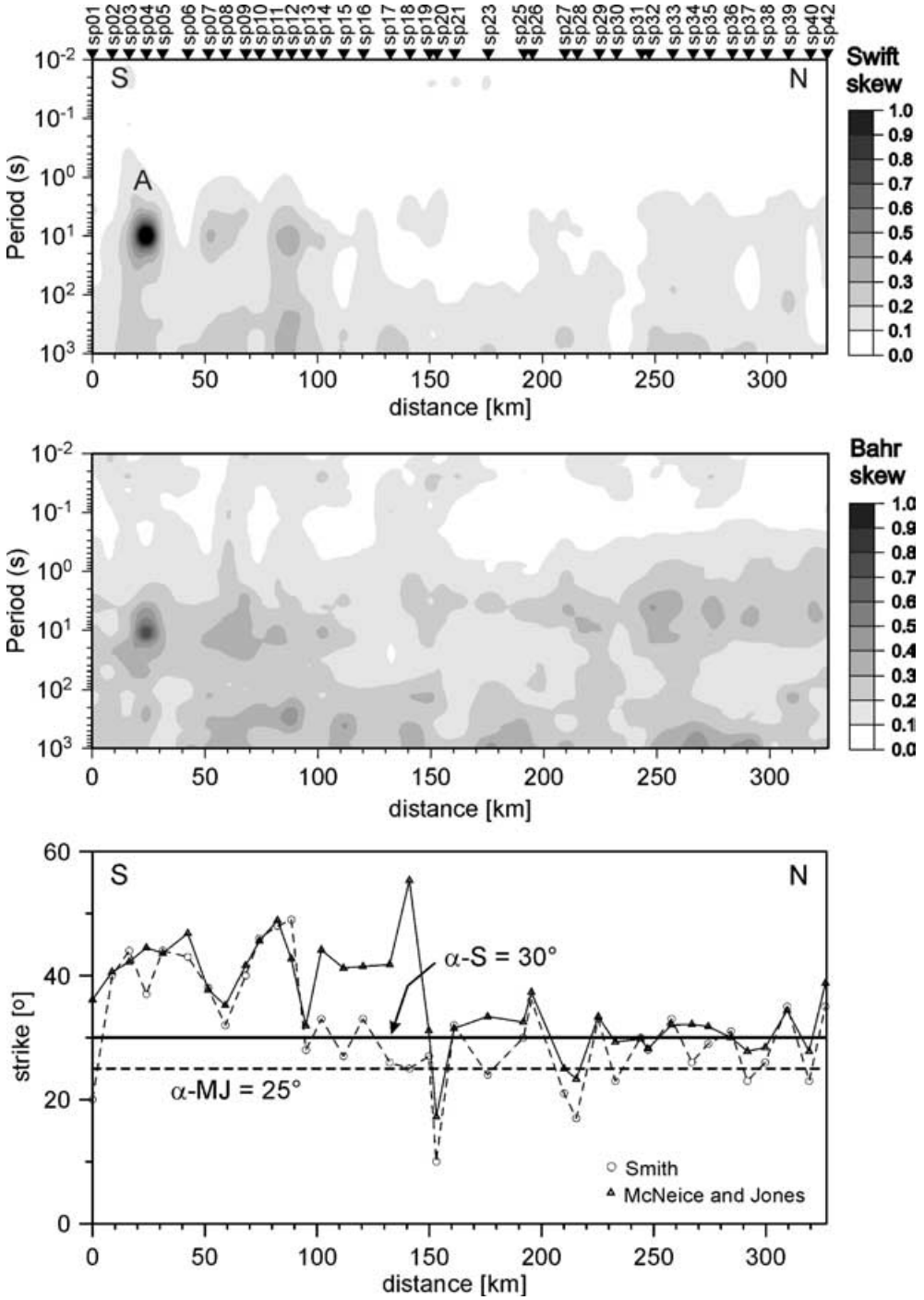

Figure 3. Swift skew-period section (top). High skew values (A) at site SP04 are due to bad data quality. Phase sensitive skew (centre). Strike directions (below) from decomposition schemes of Smith (1997) and McNeice & Jones (2001).

starting model). A minimum error floor of 15 per cent was assigned to the apparent resistivites and 1.5° to the phase data. This helps in downweighting the apparent resistivities with respect to the phases, which in turn reduces the influence of static shifts. Since this procedure led to (unrealistic) undulations of the basalt/basement interface, the weighting parameter penalizing deviation from horizontal structures was then slightly increased. The resulting model displayed in Fig. 6(a) yields an rms of 2.63; for a comparison of data and model responses see Fig. 6(b). Static shift coefficients computed from the inversion and the rms error along the profile at each station are presented in Fig. 7, showing the negligible effects of static shift on the data. The Arabian Sea is nearly 250 km west of the profile and its influence may thus be omitted for the period range considered here.

In the middle-to-deep crust six low resistive features (marked as A, B, C, D, E and F in Fig. 6a) were obtained. The structures 'B' and 'C' spatially coincide with the 'Kurduwadi feature', which is characterized by a gravity low. Anomaly 'A' is lying below Sangole gravity high. An exceptionally conductive broad anomaly 'E' is delineated at the northern part of the profile. The moderately

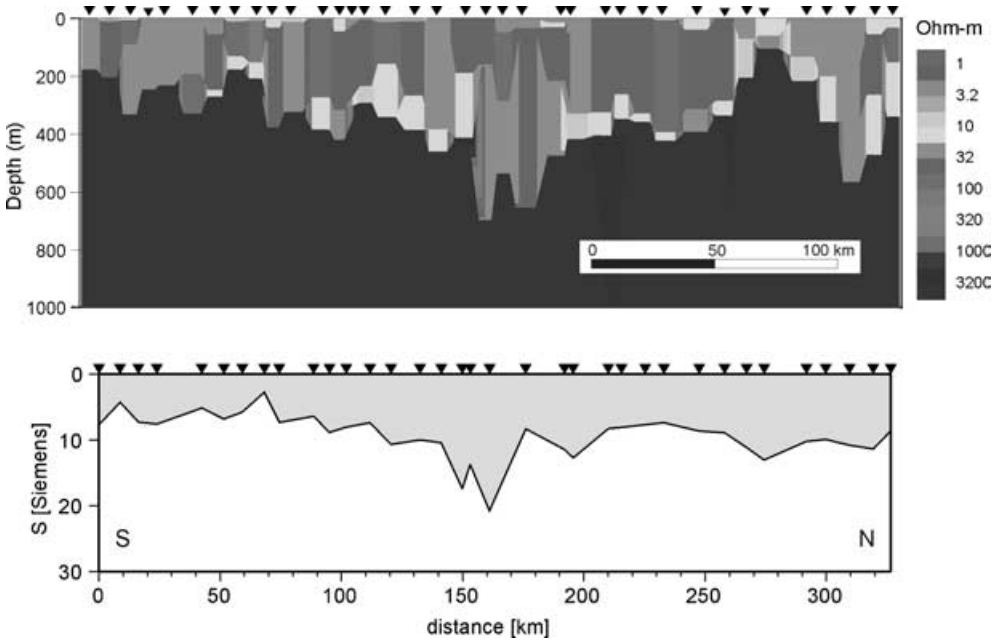

Figure 4. Top: 1-D geoelectric section derived from 1-D inversion. Bottom: Conductance of basaltic layers along the profile.

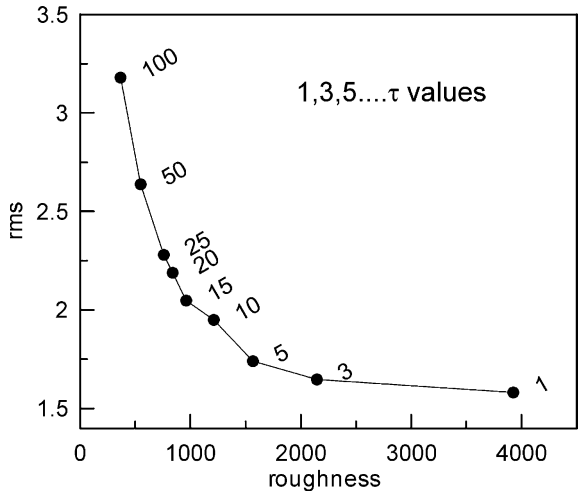

Figure 5. L-curve obtained from systematical variation of the regularization parameter.

resistive feature 'D' found below SP19 might be the trace of the Latur fault.

Additionally, TE and TM mode data were inverted independently (see Fig. 8). The rms errors for TE and TM mode inversion are 2.17 and 3.06, respectively. The results from TE mode inversion brought out the good conductor in the northern end of the profile (features 'E' and 'F') whereas the TM mode delineated the shallow conductive features (the Deccan traps).

A sensitivity analysis was carried out for the model shown in Fig. 6 to further understand the resolution of the structures. This information is used to identify those parts of the model, which are more sensitive to the data. The sensitivities generated from the algorithm were normalized by area and plotted in Fig. 9. This reveals that structures marked with A, B, C, D, E and F are well resolved and most structure below 50 km in the model centre, which represents the highly resistive upper mantle, is poorly resolved. To test the significance and resolution of some of the conductive features, their resistivity values were systematically varied and the resulting responses were compared with the ones of the model in Fig. 6, following a procedure proposed by Nolasco *et al.* (1998). The resulting model responses show that the data fit becomes worse if the resistivites of the conductive features are increased to few hundred Ωm. Fig. 10 shows the forward TE and TM responses at site SP31 with and without conductive feature E.

4 IS THE LOWER CRUST ANISOTROPIC?

The above analysis follows the standard treatment of 2-D magnetotelluric data. There are, however, several peculiar features in the data set considered here and the resulting 2-D model, which may favour a different interpretation approach. First, sounding curves are very similar and an almost constant phase split between TE and TM modes is observed over large parts of the measuring area. Second, the succession of dyke-shaped structures in the 2-D model may hide a general property of the deeper crust and/or upper mantle in the observation area. As Heise & Pous (2001) have shown, a synthetic anisotropic data set may yield dyke like structures if analysed with an isotropic inversion scheme. The macro-anisotropic character of the deeper subsurface seems even more obvious if we consider the 2-D model in Fig. 11, which was achieved with a lower regularization parameter of $\tau = 5$ (note, that this is not the preferred model, if the L-curve criterion is applied). This motivated some model computations incorporating anisotropic structures in one and two dimensions.

Electrical anisotropy is observed in many areas of the Earth's crust and there exist different models for its explanation (e.g. Cull & Spence 1985; Kellett *et al.* 1992; Mareschal *et al.* 1995; Eisel & Haak 1999; Bahr *et al.* 2000; Heise & Pous 2003; Weckmann *et al.* 2003). Electrical anisotropy was first modelled by Cull & Spence (1985); he interpreted amplitude differences between the MT impedances of two polarizations. Later Kellett *et al.* (1992) considered phase discrepancies. Eisel & Bahr (1993) and Jones *et al.* (1993) followed the concept of Kellett *et al.* (1992). They modelled the phase differences occurring in a particular period range by the

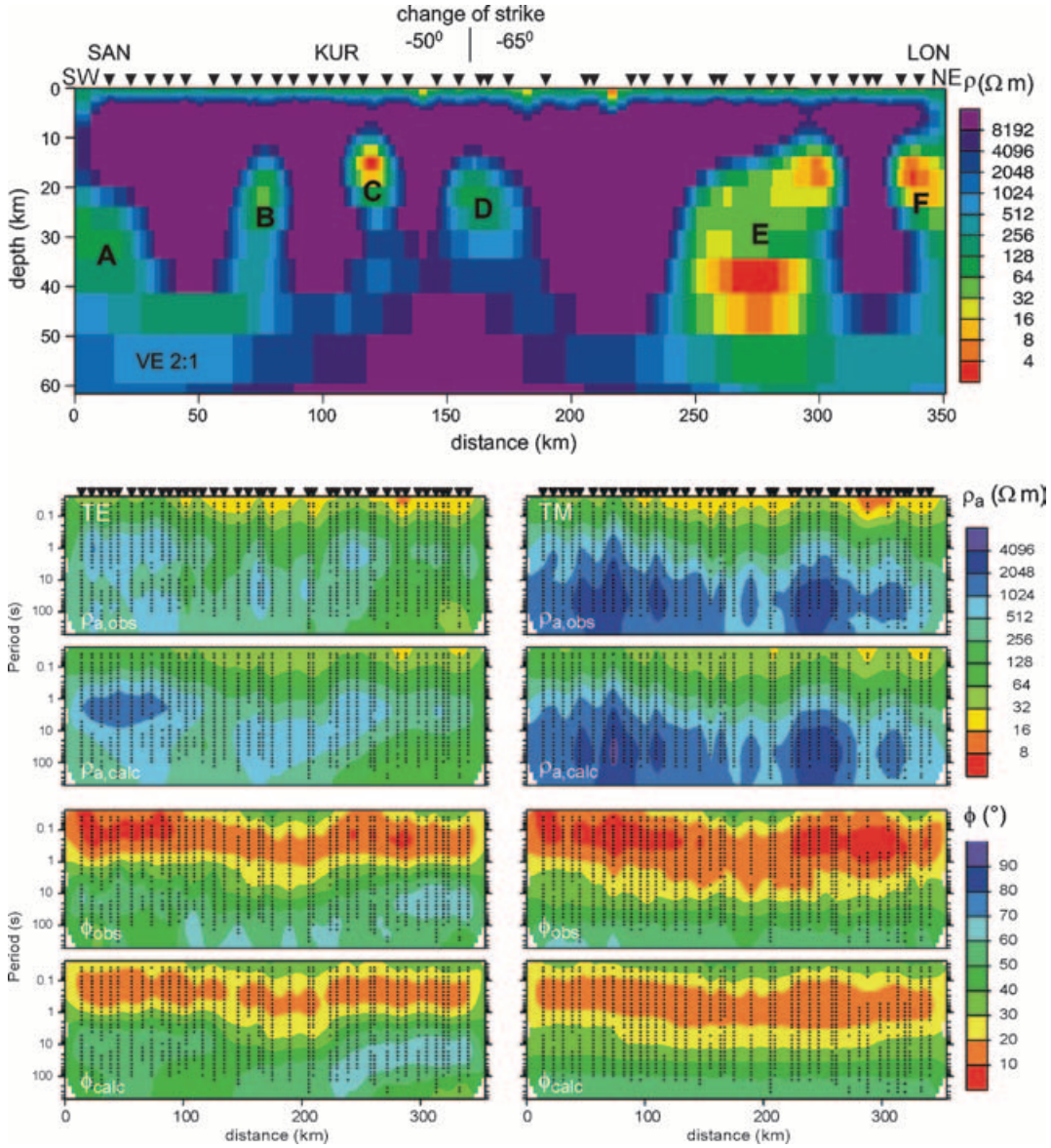

Figure 6. Top: Resistivity model derived from 2-D inversion. Mesh size is 298 × 45 cells. (a)–(f): conductive structures in the lower crust (see text). Location of major towns: SAN = Sangole, KUR = Kurduwadi, LON = Lonar. Bottom: Comparison of data and model responses. Left TE, right TM mode.

presence of an anisotropic layer in a particular depth range. Eisel & Haak (1999) modelled the observed data from the German Continental Deep Drilling Project (KTB) with an anisotropic structure considering divergence in the apparent resistivity curves and stable strike directions. By using a fractal random network Bahr (1997) demonstrated that the distribution of microcracks on small-scale results in macroscopic, anisotropic bulk conductivities.

In the anisotropic case the conductivity expands into a 3 × 3 tensor $\underline{\underline{\sigma}}$, which may be expressed by three conductivities and three angles due to symmetry against rotation:

$$\underline{\underline{\sigma}} = \begin{pmatrix} \sigma_{xx} & \sigma_{xy} & \sigma_{xz} \\ \sigma_{yx} & \sigma_{yy} & \sigma_{yz} \\ \sigma_{zx} & \sigma_{zy} & \sigma_{zz} \end{pmatrix}$$

$$= R_z(-\alpha_S)R_x(-\alpha_D)R_z(-\alpha_L)\begin{pmatrix} \sigma_1 & 0 & 0 \\ 0 & \sigma_2 & 0 \\ 0 & 0 & \sigma_3 \end{pmatrix}$$

$$\times R_z(\alpha_S)R_x(\alpha_D)R_z(\alpha_L),$$

where σ_1, σ_2 and σ_3 are conductivities in the principal directions, the angles α_S, α_D and α_L are termed strike, dip and slant, respectively, while R_x and R_z denote elementary rotation matrices (e.g. Pek & Santos 2002). Instead of one parameter in the isotropic case, now six parameters have to be analysed. For the sake of clarity, we have concentrated on adapting the three conductivities and the strike angle α_S in the modelling computations described below, mostly leaving α_D and α_L constant at 0°.

The simple structure of the data treated here suggests that an anisotropic 1-D approach may already suffice to explain general characteristics of the data. This is indeed the case, as demonstrated in Fig. 12 for a representative site (SP40). The 1-D code of Li (2000, 2002) was incorporated to calculate responses. An azimuthal anisotropy shown in Fig. 12(a) is generated by subvertical sheets, where the principal resistivities are $\rho_{\min}/\rho_{\max}$. α_S is the anisotropy strike, the angle with respect to north (or the structural strike, if a 2-D model is considered). The model (Fig. 12b) consists of four layers with the top layer representing the traps (30 Ωm), a highly

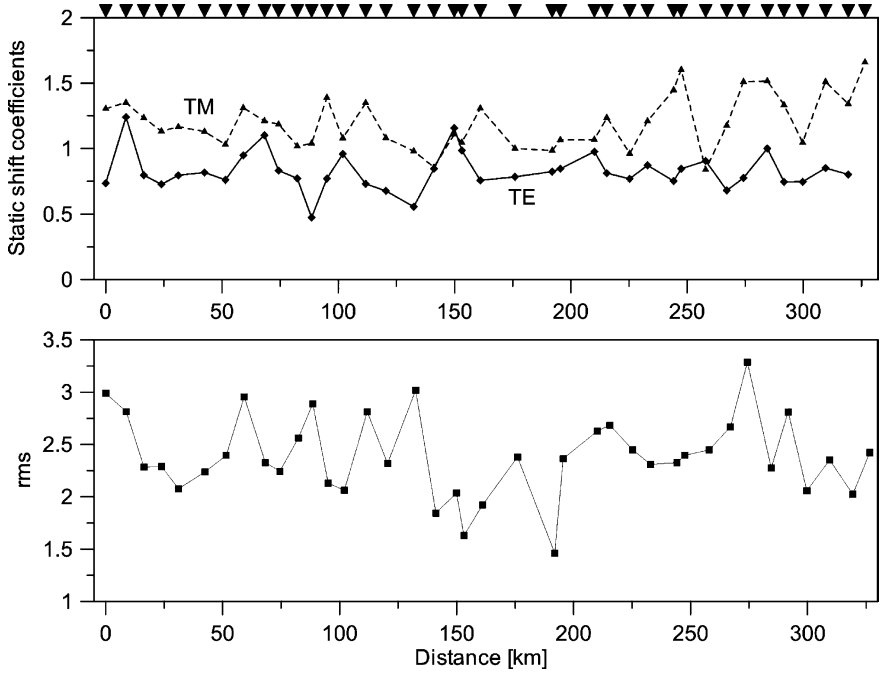

Figure 7. Top: Static shift coefficients computed from the inversion. 1 represents no static shift; Bottom: rms error along the profile at each station.

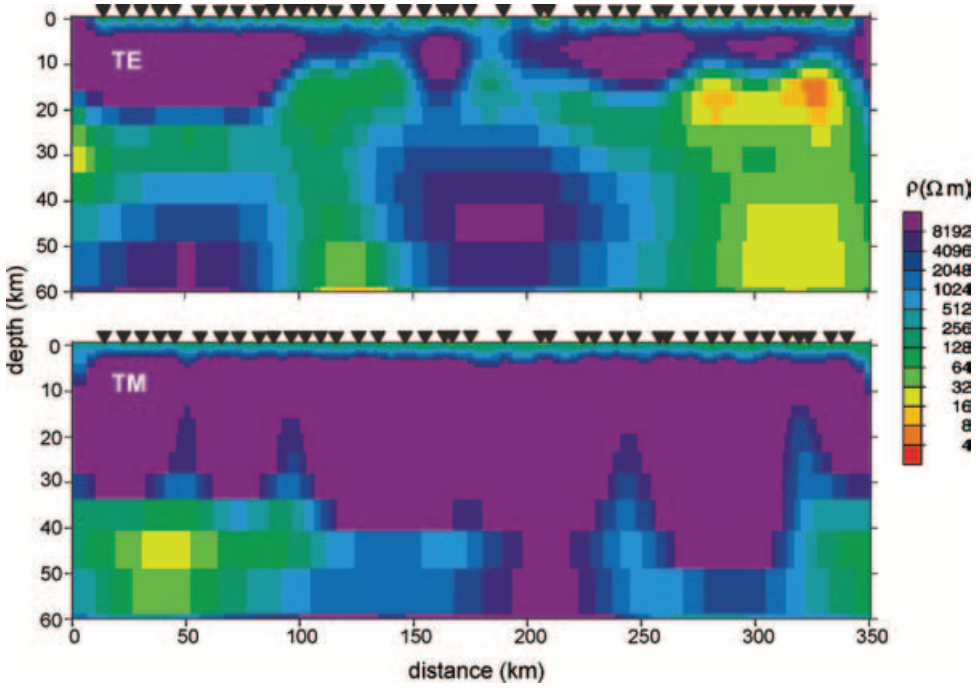

Figure 8. Models obtained after inversion of TE (top) and TM (bottom) data.

resistive basement (5000 Ωm) underlain by an anisotropic layer ($\rho_{\min}/\rho_{\max} = 10/1000$; $\alpha_S = 20^\circ$) extending to the deep crust and then the half-space of 1000 Ωm. Although the fit (shown in Fig. 12c) of both apparent resitivities and phases with the observed data is not perfect, especially at longer periods, the general features of the data are reproduced.

4.1 Influence of model parameters in 1-D

The model parameters like anisotropy strike (α_S), anisotropy ratio ($\rho_{\min}/\rho_{\max}$) and the geometry (depth, thickness) of the anisotropic layer were varied to analyse the sensitivity of model parameters. Anisotropy strike α_S of the layer was varied systematically from 0° to 90° and the resulting responses are plotted in Fig. 13(a). Until $\alpha_S = 20^\circ$ the apparent resistivities and phases behave closely to the observed data. When $\alpha_S > 20^\circ$, the *XY* phases decrease with α_S in the period range 1–200 s and *YX* phases increase in that period range. Apparent resistivity values of *XY* component increase from 1 s, whereas the *YX* components decrease. This analysis suggests a best anisotropic strike $\alpha_S = 20^\circ$. Both components (*XY* and *YX*) of apparent resistivities and phases fit with the observed data well (Fig. 13b) when the anisotropy ratio of the layer is high, that is,

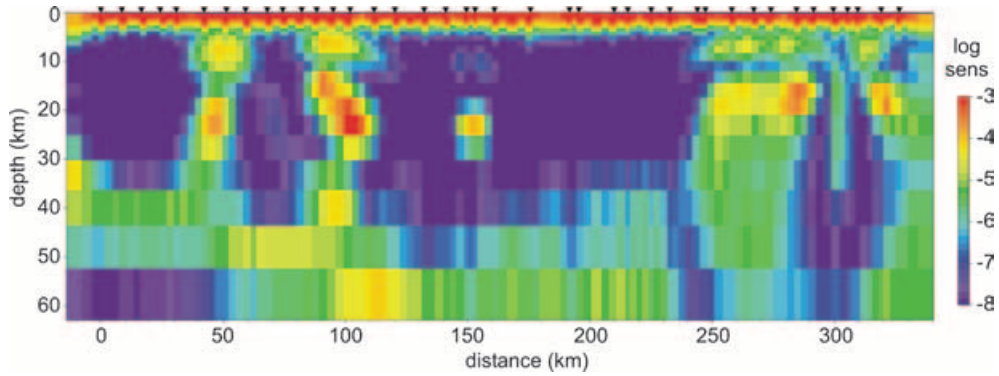

Figure 9. Sensitivities for the inversion shown in Fig. 6(a).

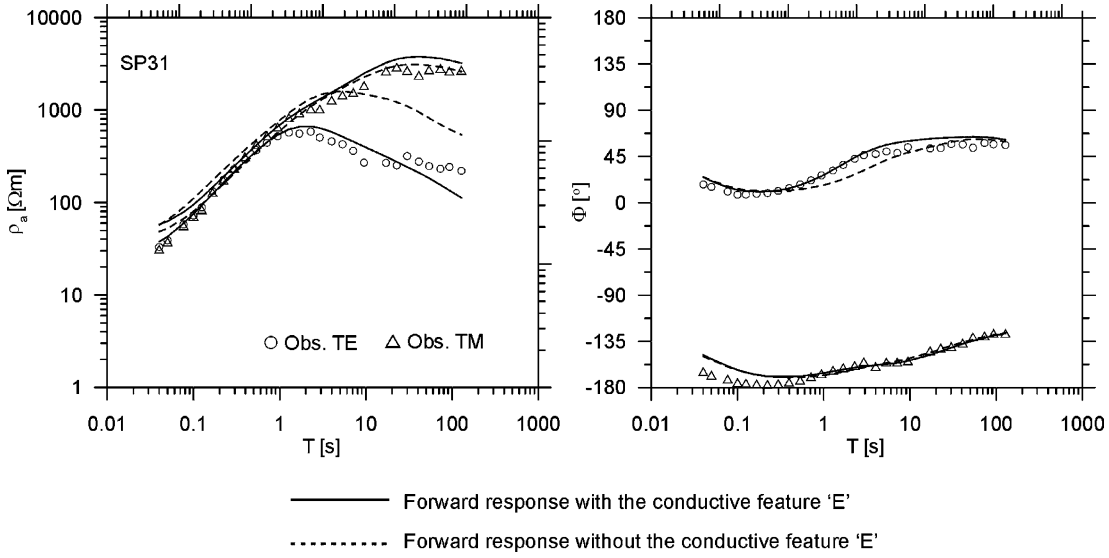

Figure 10. Forward response at site SP31 with and without the conductive feature E.

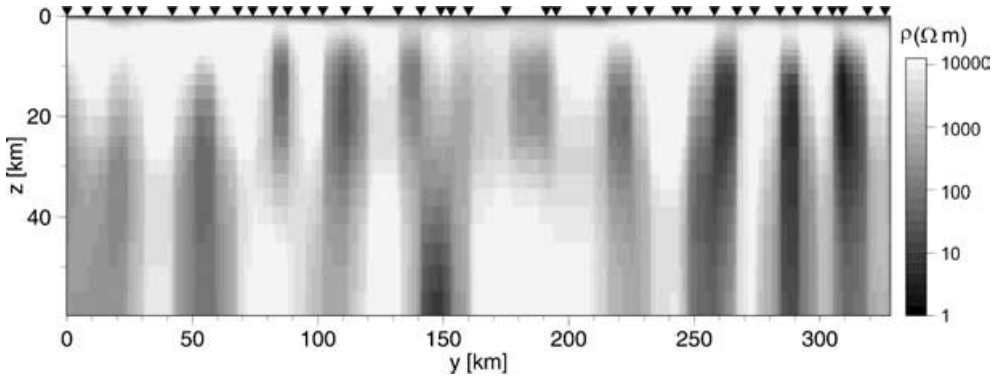

Figure 11. 2-D model after inversion with smaller regularization parameter.

$\rho_{min}/\rho_{max} = 10/1000$. It may be noted that a large deviation from the observed data is observed when the anisotropic ratio is minimum, that is, $\rho_{min}/\rho_{max} = 10/100$.

Further studies concerning depth and extent of the anisotropic layer were carried out. Modelled apparent resistivities and phases are close to the observed data when the upper boundary of the anisotropic layer is between 10–20 km (Fig. 13c). Another important aspect is to constrain the thickness of the layer. To address this problem, we have varied the thickness of the anisotropic layer from 20 to 40 km, keeping the layer top fixed at 10 km. The resulting responses are almost identical with the exception of minor differences in the *XY* component of apparent resistivities and phases at long periods (Fig. 13d). It is thus virtually impossible to resolve the bottom of the anisotropic layer if longer-period data are not available.

We also analysed a possible pseudo-anisotropy of the top layer, motivated by the observation of successive flows during creation of the Deccan traps. As expected, a good fit of the observed data at short periods is achieved when considering subhorizontal conductive sheets ($\rho_x = \rho_y \neq \rho_z$), but this may not explain the behaviour at longer periods and is not relevant for deeper structures.

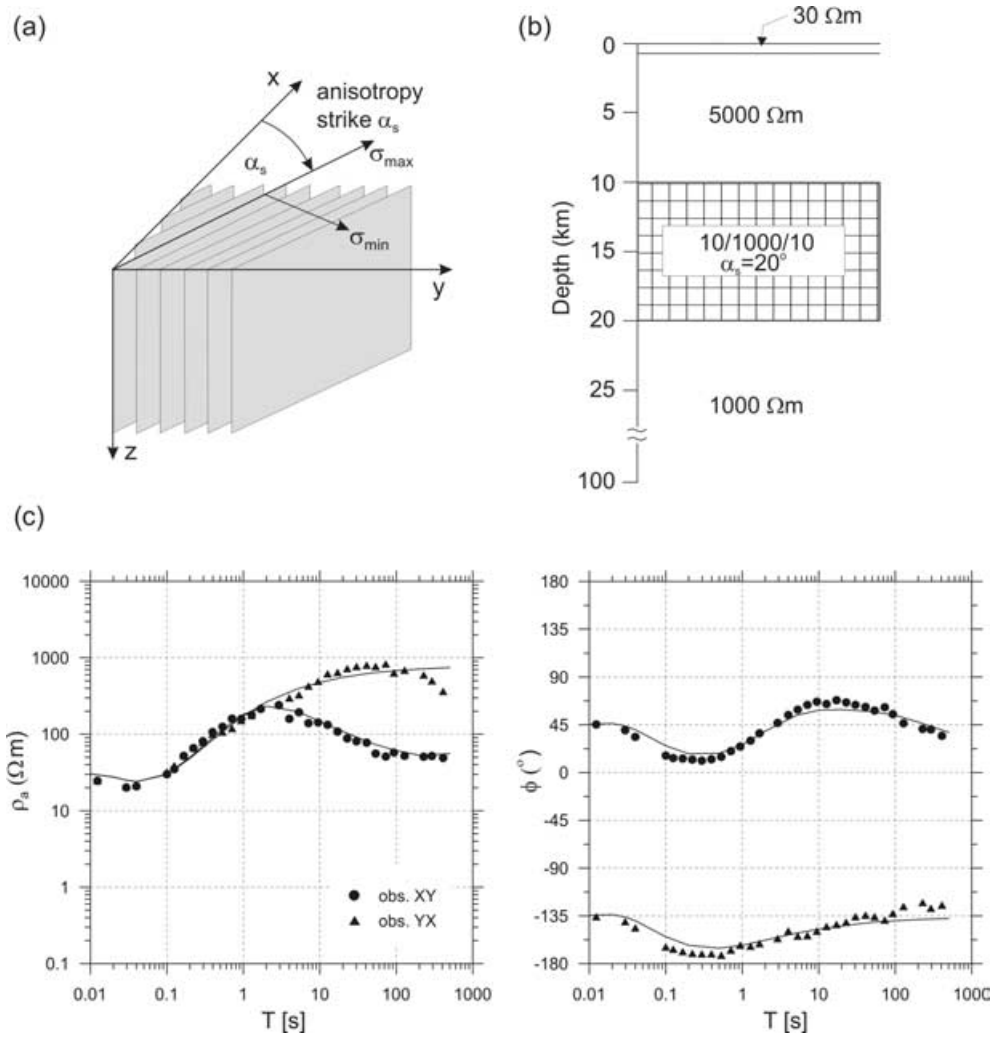

Figure 12. (a) An azimuthal anisotropic system with principal resistivities $\rho_{\min}$ and $\rho_{\max}$; (b) the initial model; (c) model responses compared with observed data.

We have thus omitted any anisotropy of the top layer in the further investigation.

4.2 2-D forward model study

To explain the whole set of transfer functions along the profile the results above have been incorporated in the construction of a 2-D anisotropic model. Pek and Verner's (1997) finite-difference forward algorithm to compute the magnetotelluric fields in 2-D with anisotropic structure was used. Again a number of computations have been carried out concerning variation of parameters, that is, resistivity ratios, strike directions and depth/thickness of anisotropic blocks. The resulting model (Fig. 14) consists of an isotropic thin layer (300–600 m) in 2-D strike direction, underlain by an isotropic layer with a resitivity of 5000 Ωm extending up to 40 km, with 3 embedded anisotropic blocks: (1) in the northern half with an anisotropy ratio of $\rho_{\min}/\rho_{\max} = 10/100$ and $\alpha_S = 20^\circ$ (2) in the southern part of the model with $\rho_{\min}/\rho_{\max} = 200/5000$ and $\alpha_S = 15^\circ$ and (3) in the centre with $\rho_{\min}/\rho_{\max} = 1000/3000$ and $\alpha_S = 20^\circ$. The isotropic lower half-space resistivity was set to $\rho = 1000$ Ωm. The grid dimension is 141 × 57 (horizontal × vertical) including 10 air layers; cell spacing is kept nearly constant around 2.5 km in horizontal direction. Fig. 14 presents the responses at several sites, compared to the corresponding observed data (in rotated coordinates) and shows that a good overall fit is achieved. As was the case for the 1-D models the lower boundary of the anisotropic blocks is poorly resolved.

Average bulk resistivities can be calculated using Kirchhoff's laws (e.g. Leibecker *et al.* 2002) parallel and perpendicular to the anisotropic structure:

$$\rho_{\parallel} = 2 \times \rho_{\min}\,\rho_{\max}/(\rho_{\min} + \rho_{\max}) \quad \text{and} \quad \rho_{\perp} = (\rho_{\min} + \rho_{\max})/2.$$

This yields conductances $S = \sigma * h$ in the conductive direction of the (middle-to-lower) crust of 72 S, 13 S and 1515 S, respectively, from south to north.

It can be concluded that the assumption of on overall macro-anisotropy of the lower crust (and possibly the upper mantle) fits the data equally well as compared to the 2-D isotropic model. This is not surprising considering that both approaches are merely different expressions of the same underlying principle, the inability to distinguish between a succession of subvertical conductive dykes and its equivalent described in terms of macro-anisotropy.

5 DISCUSSION

A regional magnetotelluric survey comprising 41 broad-band stations distributed along a 330-km-long profile extending from Sangole in the south to Partur in the north across the DVP in the

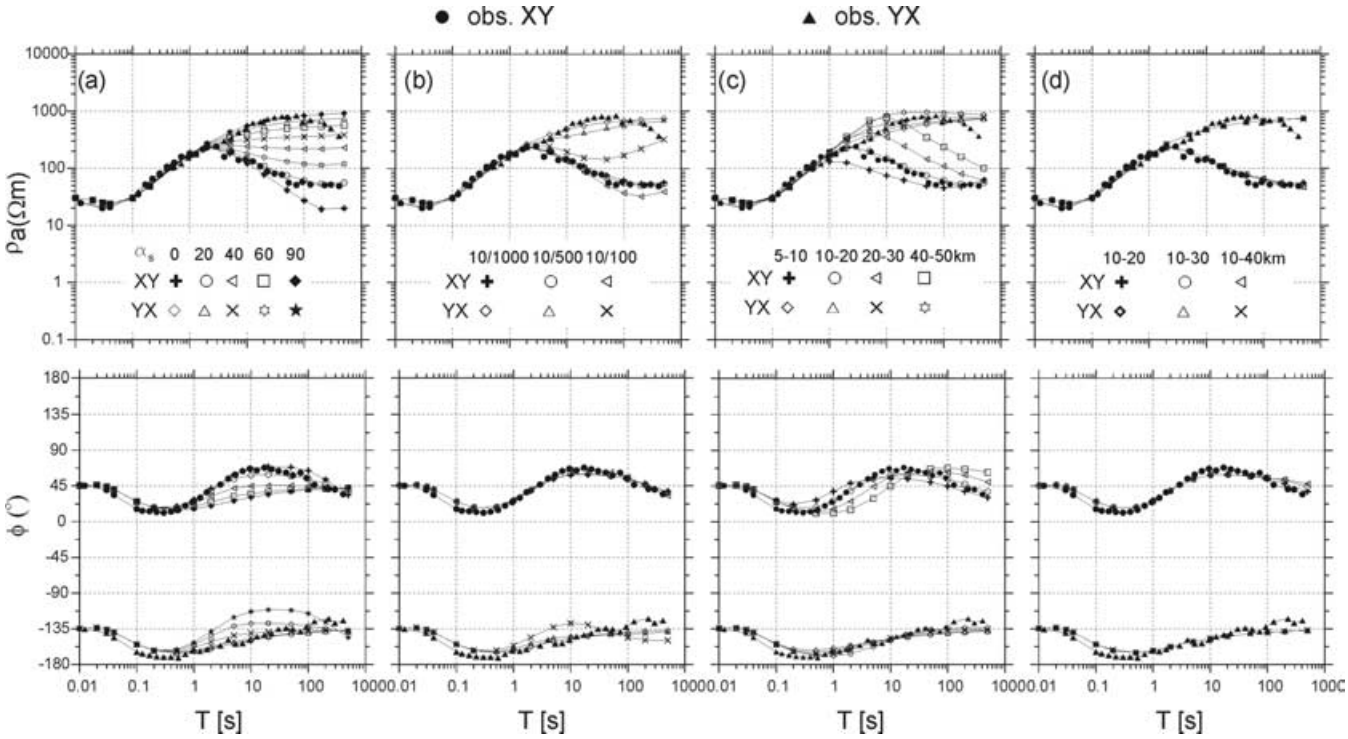

Figure 13. Apparent resistivities and phases if model parameters are varied: (a) for different anisotropic strike directions α_S; (b) for different anisotropic ratios ($\rho_{\min}/\rho_{\max}$) of the layer; (c) for different depths to the top of the anisotropic layer; (d) for different thickness of the anisotropic layer. Observed data are in the coordinate system of the 2-D model.

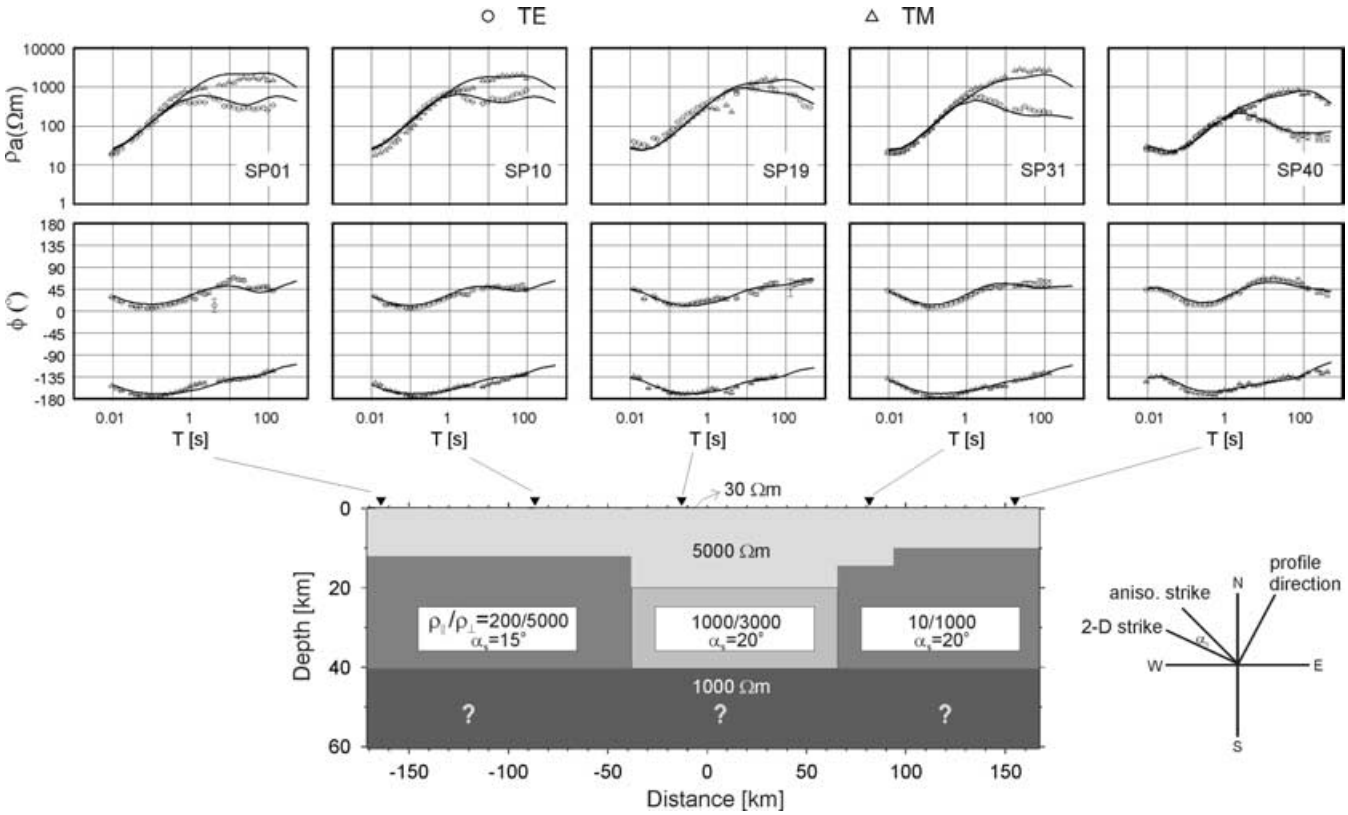

Figure 14. The anisotropic 2-D model and the responses along with data. The implied anisotropy strike α_S is the deviation from the 2-D isotropic strike, which coincides with the geological direction. '?' indicates not resolved.

Indian Peninsular shield was conducted to gain further insights into the electrical structure of the region. The study brought out thickness variations of the Deccan trap cover as well as the crustal electrical structure beneath the Deccan traps. Modelling results indicate an average thickness of 400 m for the traps, these becoming as thick as 700 m in the middle of the traverse. Deccan trap resistivities in general are found to be relatively low, falling in the range of 35–40 Ωm, which may be attributed to deep weathering as well as presence of intertrappean sediments. Detailed 2-D modelling studies led to identification of six major subvertical deep crustal conductors in the DVP, imparting a lateral electrical heterogeneous nature to the subtrappean crustal column. Modelling of the data considering an anisotropic lower crust also supports the presence of a series of conductive dykes.

Since only very few other geophysical constraints exist on the electrical nature of the lower crust beneath the DVP, interpretation of the resistivity models derived from MT data has to be somewhat tentative. Seismic studies (Kaila *et al.* 1981a,b), which inferred Moho depths of ∼40 km, are available only for areas to the west of the MT profile and thus of limited use for the actual study area. The available aeromagnetic data is also very sparse and is limited to very few profiles (Negi *et al.* 1983). Its interpretation is prone to several ambiguities particularly because of the highly variable magnetic properties of the Deccan Traps. The only additional geophysical constraint that is available, comes from detailed gravity studies along three traverses in the study area, which inferred the emplacement of low-density material in the upper crust such as granitic bodies along deep fracture/shear zones (Tiwari *et al.* 2001).

Heat flow values observed in this part of the Indian peninsular shield (Roy & Rao 2000) are low (∼40 mW m^{-2}); this is indicative of a cold and dry lithosphere underneath a major part of the DVP. Rheological models for the central Indian shield by Manglik & Singh (2002) also suggest a very low mantle derived heat flow, in accordance with the observed heat flow values. However, in the nearby region, that is, in the northern block of Southern granulite province, high (23–32 mW m^{-2}) mantle derived heat flow is reported (Ray *et al.* 2003).

For a cold and dry lithosphere, high electrical resistivities would normally be expected. Inferred conductances for the lower crust are correspondingly low (of the order of 1 S) in many parts of the world, for example, the Slave Craton (Jones 2001) or the East Indian Craton (Bhattacharya & Shalivahan 2002). However, the continental lower crust in shield regions is often electrically heterogeneous, and sometimes less resistive than originally assumed (e.g. Jones 1992). A prominent example is the Baltic Shield (e.g. Korja *et al.* 2002).

As could be seen from the modelling results of the present study, the lower crust below DVP is characterized by lateral electrical heterogeneities imparting a block structure by virtue of partitioning of a resistive lower crust by the six (A, B, C, D, E and F, see Fig. 6) major subvertical conductive zones. The resistivities of these zones are very low ∼50 Ωm for A, B, and D and even less ∼5 Ωm for the features C and E. Some of these conductive features identified, particularly A, B and C spatially coincide with prominent linear gravity anomalies cutting across the MT traverse. An immediate interpretation of the enhanced conductive zones could thus be that these may be considered representing the electrical images of crustal scale major fault/fracture zones.

Several candidates are proposed to explain such high conductive features in the crust. These include partial melt, fluids and graphites. Since partial melting can be excluded in this particular tectonic environment, fluids and solid-phase electronic conductors (e.g. graphite) remain as possible candidates to explain the observed linear conductive features in the DVP. There has been considerable debate on the cause of enhanced conductivity in the lower crust and graphite precipitated along fossil shear planes constitutes a widely accepted interpretation in stable continental regimes (e.g. Wannamaker 2000; Simpson 2001). Petrological arguments support this view, (e.g. Markl & Bucher 1998), and indicate that a connected free-fluid phase cannot exist permanently in the lower crust. Fluids are also known to play an important role in explaining crustal conductors (e.g. Unsworth *et al.* 1997, 1999; Yardley & Valley 1997; Wannamaker 2000; Li *et al.* 2003; Unsworth & Bedrosian 2004; Tank *et al.* 2005, and references there in). The source of fluids at the fault zone in mid-crustal depths could be due to dehydration of minerals during metamorphism (Byerlee 1993).

For the anomalies A, B and D the modelled anomalous resistivities are of the order of ∼50 Ωm; thus only approximately 1–2 per cent of (interconnected) fluids are enough to lower the crustal resistivities to this level, and even lesser percentage, if graphite (with a conductivity in the range of 10 000–1 000 000 S m^{-1}) is considered. For the more conductive (∼5 Ωm) structures C and E (and F, which is at the end of the profile and hence cannot be considered as resolved), however, a first-order approximation for example, considering the upper Hashin–Shtrikman bound with resistivities of 0.1 Ωm for the conductive (fluid) and 10 000 Ωm for the resistive phase requires a ∼4 per cent interconnected pore space to match the observed resistivities of ∼5 Ωm. This value seems unrealistically high, and although the necessary pore space may be considerably smaller if higher fluid conductivities are assumed, but this is almost automatically assured if graphite is assumed to constitute the conductive phase. The conductor E, which is located deep in the lower crust, as compared to other conductors, might thus belong to the graphite environment, while the conductors A, B, C and D can be attributed to fluid enrichment in the fracture zones.

These faults hidden underneath the Deccan trap cover might represent Precambrian weak zones and might play a considerable role in shaping its seismotectonic character. These subtrappean-hidden faults, inferred to be fluid enriched, may possibly be reactivated under the influence of the ambient stress field in the Indian plate due to its northward movement and its subsequent collision with the Asian plate at the Himalayas. The study area lies in the southwestern part of the 'Mid-continent stress province', defined by Gowd *et al.* (1992), where the maximum stress direction is NNE–NE deduced from borehole breakouts, hydrofracture measurements and SH_{max} observations of regional earthquakes. The strike of conductive features (both in isotropic and anisotropic models) cuts across the maximum stress direction of this mid-continental stress province and hence the increased vulnerability of these fluid enriched fault/fracture zones to become seismically active.

ACKNOWLEDGMENTS

The study was funded by the Department of Science and Technology (DST), Government of India. We thank V. P. Dimri, the Director of NGRI for constant encouragement and support. R. S. Sastry, D. N. Murty, M. V. C. Sarma, K. Veeraswamy and T. Srinivasulu participated in the field campaign. We express our gratitude to Josef Pek for providing the 2-D forward code. Thanks are also due to Yuguo Li for his 1-D anisotropic forward program and useful discussions. We also benefited from discussions with Ulrich Schmucker and Karsten

Bahr and the comments from P. Wannamaker and an anonymous reviewer. We thank the editor Martyn Unsworth for constructive suggestions. B. Prasanta K. Patro thanks DST for the BOYSCAST fellowship to the FU Berlin.

REFERENCES

Bahr, K., 1997. Electrical anisotropy and conductivity distribution functions of fractal random networks and of the crust: the scale effect of connectivity, *Geophys. J. Int.,* **130,** 649–660.

Bahr, K., 1988. Interpretation of the magnetotelluric impedance tensor: regional induction and local distortion, *J. Geophys.,* **62,** 119–127.

Bahr, K., Bantin, M., Jantos, C., Schneider, E. & Storz, W., 2000. Electrical anisotropy from electromagnetic array data: implications for the conduction mechanism and for distortion at long periods, *Phys. Earth planet. Inter.,* **119,** 237–257.

Berdichevsky, M.N. & Dimitriev, V.I., 2002. Magnetotellurics in the context of ill-posed problems, Society of Exploration Geophysicists, Tulsa, 215 pp.

Berdichevsky, M.N. & Dmitriev, V.I., 1976. Basic principles of interpretation of magnetotelluric sounding curves, in *Geoelectric and Geothermal Studies*, pp. 165–221, ed. Adam, A., *KAPG Geophysics Monographs,* Akademiai Kiado, Budapest.

Bhaskar Rao, K.V.S., Jagannatha Rao, K. & Satyanarayana, K.V., 1995. Geophysical studies along Kurduwadi-Latur section to delineate structures below Deccan Traps, *Geol. Surv. India Spec. Publ.,* **27,** 91–98.

Bhattacharya, B.B. & Shalivahan, 2002. The electric moho underneath Eastern Indian Craton, *Geophy. Res. Lett.,* **29,** 10, doi:10.1029/2001GL014062.

Biswas, S.K., 1982. Rift basins in western margin of India and their hydrocarbon prospects with special reference to Kutch basin, *Am. Assoc. Petr. Geol. Bull.* **66,** 1497–1513.

Biswas, S.K., 1987. Regional tectonic framework, structure and evolution of the western maginal basins of India, *Tectonophysics,* **135,** 307–327.

Byerlee, J., 1993. Model for episodic flow of high-pressure water in fault zones before earthquakes, *Geology,* **21,** 303–306.

Courtillot, V., Besse, J., Vandamme, D., Montigny, R., Jaeger, J.J. & Cappetta, H., 1986. Deccan flood baslts at the Creataceous/Tertiary boundary?, *Earth planet. Sci. Lett.,* **80,** 361–374.

Cull, J.P. & Spence, A.G., 1985. Magnetotelluric soundings over a Precambrian boundary in Australia, *Geophys. J. R. astr. Soc.,* **80,** 661–675.

Deshmukh, S.S. & Sehgal, M.N., 1988. Mafic dyke swarms in Deccan Volcanic Province of Madhya Pradesh and Maharastra, in *Deccan Flood Basalts*, Vol. 10, pp. 323–340, ed. Subbarao, K.V., Memoir Geol. Soc, India.

Duncan, R.A. & Pyle, D.G., 1988. Rapid eruption of Deccan Flood Basalts at the Cretaceous-Tertiary boundary, *Nature,* **333,** 841–843.

Eisel, M. & Haak, V., 1999. Macro-anisotropy of the electrical conductivity of the crust: a magnetotelluric study of the German Continental Deep Drilling site (KTB), *Geophys. J. Int.,* **136,** 109–122.

Eisel, M. & Bahr, K., 1993. Electrical anisotropy in the lower crust of British Columbia: an interpretation of a magnetotelluric profile after tensor decomposition, *J. Geomag. Geoelectr.,* **45,** 115–126.

Frost, B.R., Fyfe, W.S., Tazaki, K. & Chan, T., 1989. Grain-boundary graphite in rocks and implications for high electrical conductivity in the lower crust, *Nature,* **340,** 134–136.

Geotools, 1997. *Users guide, Geotools Corporation*, Texas, USA, p. 448.

Gokarn, S.G., Rao, C.K., Singh, B.P. & Nayak, P.N., 1992. Magnetotelluric studies across the Kurduwadi gravity feature, *Phys. Earth planet. Inter.,* **72,** 58–67.

Gokarn, S.G., Rao, C.K., Gupta, G., Singh, B.P. & Yamashita, M., 2001. Deep crustal structure in central India using magnetotelluric studies, *Geophys. J. Int.,* **144,** 685–694.

Gowd, T.N., Srirama Rao, S.V. & Gaur, V.K., 1992. Tectonic stress field in the Indian subcontinent, *J. geophys. Res.,* **97**(B8), 11 879–11 888.

Gupta, H.K. & Dwivedy, K.K., 1996. Drilling at Latur earthquake region exposes a Peninsular Gneiss basement, *J. Geol. Soc. India,* **47,** 129–131.

Gupta, H.K, Sarma, S.V.S., Harinarayana, T. & Virupakshi, G., 1996. Fluids below hypocentral region of the Latur earthquake, India, *Gephys. Res. Lett.,* **23,** 1569–1572.

Gupta, H.K., Mohan, I., Rastogi, B.K., Rao, M.N. & Ramakrishna Rao, C.V., 1993. A quick look at the Latur earthquake of 30th Sept., 1993, *Curr. Sci.,* **65,** 517–520.

Gupta, H.K., Mandal, P. & Rastogi, B.K., 2002. How long will triggered earthquakes at Koyna, India continue?, *Cur. Sci.,* **82,** 202–210.

Hansen, P.C., 1998. *Rank Deficient and Discrete Ill-Posed Problems, Numerical Aspects of Linear Inversion*, SIAM, Philadelphia, Pennsylvania p. 247.

Heise, W. & Pous, J., 2001. Effects of anisotropy on the two-dimensional inversion procedure, *Geophys. J. Int.,* **147,** 610–621.

Heise, W. & Pous, J., 2003. Anomalous phases exceeding 90° in magnetotellurics: anisotropic model studies and a field example, *Geophys. J. Int.,* **155,** 308–318.

Johnston, A.C. & Kanter, L.R., 1990. Earthquakes in stable continental crust, *Sci. Amer.,* **262,** 68–75.

Jones, A.G., 1992. Electrical conductivity of the continental lower crust, in *Continental Lower Crust*, p. 502, eds Fountain, D.M., Arculus, R. & Key, R.W., 81–143, Elsevier, Amsterdam.

Jones, A.G., Groom, R.D. & Kurtz, R.D., 1993. Decomposition and modelling of the BC 87 data set, *J. Geomag. Geoelectr.,* **45,** 1127–1150.

Jones, A.G., Ferguson, I.J., Chave, A.D., Evans, R.L. & McNeice, G.W., 2001. The Electric Lithosphere of the Slave Craton, *Geology,* **29,** 423–426.

Kaila, K.L., Reddy, P.R., Dixit, M.M. & Lazrenko, M.A., 1981a. Deep crustal structure at Koyna, Maharashtra indicated by Deep Seismic Soundings, *J. Geol. Soc. India,* **22,** 1–16.

Kaila, K.L., Murty, P.R.K., Rao, V.K. & Kharetchko, G., 1981b. Crustal structure from deep seismic sounding along the KOYII (Kelsi-Loni) profile in the Deccan trap area, India, *Tectonophysics,* **73,** 365–384.

Kailasam, L.N., Murty, B.G.K. & Chayanulu, A.Y.S.R., 1972. Regional gravity studies of the Deccan Trap areas of Peninsular India, *Current Science,* **41,** 403–407.

Kailasam, L.N., Reddy, A.G.B., Rao, Joga, Sathyamurthy, K. & Murthy, B.S.R., 1976. Deep electrical resistivity soundings in Deccan Trap region, *Current Science,* **45,** 4–16.

Kellett, R.L., Mareschal, M. & Kurtz, R.D., 1992. A model of lower crustal electrical anisotropy for the Pontiac subprovince of the Canadian Shield, *Geophys. J. Int.,* **3,** 141–150.

Korja, T. *et al.*, 2002. Crustal conductivity in Fennoscandia—a compilation of a database on crustal conductance in the Fennoscandian Shield, *Earth Planets Space,* **54,** 535–558.

Krishna Brahmam, N. & Negi, J.G., 1973. Rift valleys beneath the Deccan Trap (India), *Geophys. Res. Bull.,* **11,** 207–237.

Leibecker, J., Gatzemeier, A., Hönig, M., Kuras, O. & Soyer, W., 2002. Evidence of electrical anisotropic structures in the lower crust and the upper mantle beneath the Rhenish Shield, *Earth planet. Sci. Lett.,* **202,** 289–302.

Li, Y., 2000. Numerische Modellierungen von elektromagnetischen Feldern in 2- und 3-dimensionalen anisotropen Leitfähigkeitsstrukturen der Erde nach der Methode der Finiten Elemente, *PhD thesis*, Univ. of Göttingen, Germany.

Li, Y., 2002. A finite element algorithm for electromagnetic induction in two-dimensional anisotropic conductivity structures, *Geophys. J. Int.,* **148,** 389–401.

Li, S., Unsworth, M.J., Booker, J.R., Wei, W., Tan, H. & Jones, A.G., 2003. Partial melt or aqueous fluids in the Tibetan crust: Constraints from INDEPTH magnetotelluric data, *Geophys. J. Int.,* **153,** 289–304.

Manglik, A. & Singh, R.N., 2002. Thermomechanical structure of the central Indian shield: constraints from deep crustal seismicity, *Current science,* **82,** 1151–1157.

Mareschal, M., Fyfe, W.S., Percival, J. & Chan, T., 1992. Grain boundary graphite in Kapuskasing gneisses and implications for lower-crustal conductivity, *Nature,* **357,** 674–677.

Mareschal, M., Kennett, R.L., Kurtz, R.D., Ludden, J.N. & Bailey, R.C., 1995. Archean cratonic roots, mantle shear zones, and deep electrical anisotropy, *Nature,* **373,** 134–137.

Markl, G. & Bucher, K., 1998. The presence and composition of fluids in the lower crust as inferred from metamorphic salt in granulites, *Nature,* **391,** 781–783.

McNeice, G.W. & Jones, A.G., 2001. Multisite, multifrequency tensor decomposition of magnetotelluric data, *Geophysics,* **66,** 158–173.

Negi, J.G., Agrawal, P.K. & Rao, K.N.N., 1983. Three-dimensional model of the Koyna area of Maharashtra state (India) based on the spectral analysis of aeromagnetic data, *Geophysics,* **48,** 964–974.

Nolasco, R., Tarits, P., Filloux, J.H. & Chave, A.D., 1998. Magnetotelluric imaging of the Society Island hotspot, *J. geophys. Res.,* **103,** 30 287–30 309.

Pek, J. & Verner, T., 1997. Finite-difference modeling of magnetotelluric fields in two-dimensional anisotropic media, *Geophys. J. Int.,* **128,** 505–521.

Pek, J. & Santos, F.A.M., 2002. Magnetotelluric impedances and parametric sensitivities for 1-D anisotropic layered media, *Computers and Geosciences,* **28**(8), 939–950.

Patro, B.P.K., 2002. A magnetotelluric study of crustal geoelectric structure in western India in relation to seismotctonics of the Deccan trap region, *PhD thesis*, Osmania University, Hyderabad.

Patro, B.P.K., Harinarayana, T., Sastry, R.S., Madhusudan Rao Manoj, C., Naganjaneyulu, K. & Sarma, S.V.S., 2005. Electrical imaging of Narmada-Son Lineament Zone, Central India from magnetotellurics, *Phys. Earth. planet. Inter.,* **148,** 215–232.

Prieto, C., Perkins, C. & Berkman, E., 1985. Columbia River Basalt Plateau—An integrated approach to interpretation of basalt-covered areas, *Geophysics,* **50,** 2709–2719.

Rajan, M. & Anand, S.P., 2003. Central Indian tectonics revisited using aeromagnetic data, *Earth Planets Space,* **55**, (e-Letter), e1-e4.

Ranganayaki, R.P., 1984. An interpretive analysis of magnetotelluric data, *Geophysics,* **49,** 1730–1748.

Ray, L., Kumar, P.S., Reddy, G.K., Rao, G.V., Srinivasan, R. & Rao, R.U.M., 2003. High mantle heat flow in a Precambrian granulite province: Evidence from South India, *J. geophys. Res.,* **108**(B2), 2084, doi:10.1029/2001JB000688.

Rodi, W. & Mackie, R.L., 2001. Nonlinear conjugate gradients algorithm for 2-D magnetotelluric inversion, *Geophysics,* **66,** 174–187.

Roy, S. & Rao, R.U.M., 2000. Heat flow in the Indian shield, *J. geophys. Res.,* **105,** 25 587–25 604.

Sarma, S.V.S., Patro, B.P.K., Harinarayana, T., Veeraswamy, K., Sastry, R.S. & Sarma, M.V.C., 2004. A magnetotelluric (MT) study across the Koyna seismic zone, Western India: evidence for block structure, *Phys. Earth planet. Inter.,* **142**(1–2), 23–36.

Sarma, S.V.S. *et al.*, 1994. A wide band magnetotelluric study of the Latur earthquake region, Maharashtra, India, in *Latur Earthquake*, Vol. 35, pp. 101–118, ed. Gupta, H.K., *Memoir Geol. Soc,* India,

Schwalenberg, K., Rath, V. & Haak, V., 2002. Sensitivity studies applied to a two-dimensional resistivity model from the Central Andes, *Geophys. J. Int.,* **150,** 673–686.

Sheth, H.C. & Chandrasekharam, D., 1997. Plume-rift interaction in the Deccan volcanic province, *Phys. Earth planet. Inter.,* **99,** 179–187.

Simpson, F., 2001. Fluid trapping at the brittle-ductile transition re-examined, *Geofluids,* **1,** 123–136.

Smith, J.T., 1997. Estimating galvanic-distortion magnetic fields in magnetotellurics, *Geophys. J. Int.,* **130,** 65–72.

Swift, C.M., 1967. A magnetotelluric investigation of electrical conductivity anomaly in the southwestern United States, 1967, *PhD thesis*, MIT, Cambridge, Massachusetts.

Tank, S.B. *et al.*, 2005. Magnetotelluric imaging of the fault rupture area of the 1999 Izmit (Turkey) earthquake, *Phys. Earth planet. Inter.,* **150,** 213–225.

Tiwari, V.M., Vyaghraswara Rao, M.B.S. & Mishra, D.C., 2001. Density inhomogeneities beneath Deccan Volcanic Province, India, as derived from gravity data, *J. Geodyn.,* **31,** 1–17.

Unsworth, M. & Bedrosian, P.A., 2004. Electrical resistivity structure at the SAFOD site from magnetotelluric exploration, *Geophys. Res. Lett.,* **31,** L12S05, doi:10.1029/2003GL019405.

Unsworth, M.J., Egbert, G.D. & Booker, J.R., 1999. High-resolution electromagnetic imaging of the San Andreas fault in Central California, *J. geophys. Res.,* **104,** 1131–1150.

Unsworth, M.J., Malin, P.E., Egbert, G.D. & Booker, J.R., 1997. Internal structure of the San Andreas fault zone at Parkfield, California, *Geology,* **25,** 359–362.

Wannamaker, P.E., 2000. Comment on "The petrologic case for a dry lower crust" by Bruce W.D. Yardley and John W. Valley, *J. geophys. Res.,* **105**(B3), 6057–6064.

Warren, R.K. & Srnka, L.J., 1992. Exploration in the basalt-covered areas of the Columbia River Basin, Washington, using electromagnetic array profiling (EMAP), *Geophysics,* **57,** 986–993.

Weckmann, U., Ritter, O. & Haak, V., 2003. Images of the magnetotelluric apparent resistivity tensor, *Geophys. J. Int.,* **155,** 456–468.

Yardley, B.W.D. & Valley, J.W., 1997. The petrologic case for a dry lower crust, *J. geophys. Res.,* **102,** 12 173–12 185.

Zhamaletdinov, A.A., 1996. Graphite in the Earth's crust and electrical conductivity anomalies, Izvestiya, *Phys. Solid Earth,* **32,** 272–288.